

An Auto-Zero-Voltage-Switching Quasi-Resonant LED Driver With GaN FETs and Fully Integrated LED Shunt Protectors

Lisong Li, *Student Member, IEEE*, Yuan Gao^{ID}, *Member, IEEE*, Huaxing Jiang, *Student Member, IEEE*,

Philip K. T. Mok^{ID}, *Fellow, IEEE*, and Kei May Lau, *Fellow, IEEE*

Abstract—An auto-zero-voltage-switching (ZVS) quasi-resonant LED driver with gallium nitride (GaN) FETs for general lighting applications is presented. The proposed LED driver switches at high frequency to minimize the inductors to microhenry range. ZVS can be automatically achieved with the proposed controller to eliminate switching loss. The GaN FETs enable high-frequency operation and improve the power efficiency. A fully integrated LED shunt protector is proposed to bypass the failed LEDs in series-connected LED strings. The overall lifetime of the LED strings can be improved, and the maintenance cost can be reduced. The characteristics of the ZVS quasi-resonant LED driver with small inductors and the conditions for ZVS are also discussed in detail. The LED driver is fabricated with a 0.35- μm 120-V high-voltage process. It can provide up to 25-W power to the LED with $2 \times 3.3 \mu\text{H}$ inductors and achieves 91.4% peak efficiency and a 0.973 peak power factor from 60-Hz 100- to 120-V_{ac} input.

Index Terms—AC-DC, gallium nitride (GaN), high frequency, LED driver, LED protection, open circuit, quasi-resonant, small inductor, zero-voltage switching (ZVS).

I. INTRODUCTION

LEDs have many advantages over traditional light sources, including good efficacy, long lifetime, and environmentally friendly properties [1]. However, the cost of LED systems is usually higher than that of traditional light sources. As essential off-chip components in the LED driver, the inductors in high-voltage applications are usually hundreds of microhenry [2]–[5], meaning that they are not only expensive but also take up a lot of spaces. Therefore, reducing the value of the inductors of LED drivers will contribute to

Manuscript received April 30, 2017; revised August 23, 2017 and November 10, 2017; accepted December 4, 2017. Date of publication January 4, 2018; date of current version February 21, 2018. This paper was approved by Associate Editor Yogesh Ramadas. This work was supported by the Research Grants Council of the Hong Kong Special Administrative Region Government through the Theme-based Research Scheme under Grant T23-612/12-R. (*Corresponding author: Philip K. T. Mok*)

L. Li was with the Department of Electronic and Computer Engineering, The Hong Kong University of Science and Technology, Hong Kong. He is now with CoilEasy Technologies, Shenzhen 518031, China (e-mail: lliai@connect.ust.hk).

Y. Gao, H. Jiang, P. K. T. Mok, and K. M. Lau are with the Department of Electronic and Computer Engineering, The Hong Kong University of Science and Technology, Hong Kong (e-mail: ygaoad@connect.ust.hk; hjiangab@connect.ust.hk; eemok@ust.hk; eekmlau@ust.hk).

Color versions of one or more of the figures in this paper are available online at <http://ieeexplore.ieee.org>.

Digital Object Identifier 10.1109/JSSC.2017.2783685

the cost and size reduction of LED systems [6]. A silicon-embedded inductor in the microhenry range is reported in [7], which provides a solution to integrating the inductors with the driver circuits. However, the inductance is still about 100 times smaller than the required inductance in commercial LED drivers. Increasing the switching frequency can reduce required inductance, but high switching frequency also leads to large switching loss. The switching loss due to charging and discharging of the parasitic drain capacitance of the power switch can be expressed as

$$P_s = \frac{1}{2} C_{d,\text{energy}}(V_{IN}) V_{IN}^2 f_s \quad (1)$$

where $C_{d,\text{energy}}(V_{IN})$ is the energy-related drain capacitance of the power switch when the voltage across C_d is V_{IN} , V_{IN} is the input voltage of the LED system, and f_s is the switching frequency. Considering an LED driver switching at 5 MHz, with input voltage of 160 V and drain capacitance of 60 pF, switching loss of 3.84 W will be induced and efficiency will be severely degraded. Therefore, it is challenging to reduce the inductor value and maintain a good performance at the same time.

Liu and Lee [8] proposed a synchronous LED driver that uses an adaptive resonant timing control technique to achieve zero-voltage switching (ZVS) of both the high- and low-side power switch. The LED driver can operate at up to 2.2 MHz with L of 10–39 μH . However, the LED driver requires a high-voltage PMOS that is not common in many fabrication processes. Besides this, the maximum input voltage for this design is 115 V_{dc}, and thus it cannot be used in off-line applications. The quasi-resonant LED drivers [9]–[13] shown in Fig. 1 can effectively reduce the inductance with high switching frequency operation, and the switching loss is eliminated by ZVS. Compared with the buck converter, a small inductor L_r is added in the power stage. During the OFF time of the power switch Q, L_r resonates with C_d , and the voltage across C_d rises to a high voltage and then drops to zero before Q is turned on. Consequently, the switching loss due to C_d can be eliminated and high power efficiency can be maintained when operating at high frequency. The steady-state characteristics of ZVS quasi-resonant converters have been discussed in [9]. According to their analysis, L , C , and the LEDs are simplified as a constant current source, as shown

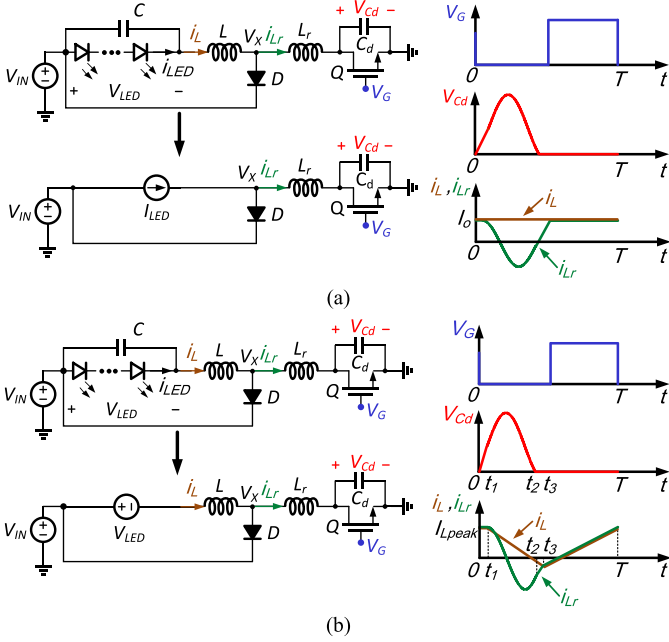


Fig. 1. Topology and steady-state operation principles of ZVS quasi-resonant LED driver. (a) Model for large inductors. (b) Model for any inductors.

in Fig. 1(a). The corresponding conversion ratio equation is

$$\frac{V_{LED}}{V_{IN}} = 1 - \frac{f_s}{2\pi f_r} \left(\arcsin \beta + \frac{\beta}{2} + \frac{1 + \sqrt{1 - \beta^2}}{\beta} + \pi \right) \quad (2)$$

where f_s is the switching frequency, I_{LED} is the current of the LEDs, and f_r and β are defined as

$$f_r = \frac{1}{2\pi\sqrt{C_d L_r}}, \quad \beta = \frac{V_{IN}}{I_{LED}} \sqrt{\frac{C_d}{L_r}}. \quad (3)$$

This simplification is only valid when L is large enough, and the resulting current ripple of L can be neglected. However, a small L is preferable for its smaller size and lower cost. As L is reduced to microhenry range, the inductor current ripple becomes large, and this assumption does not hold anymore. Under such circumstances, (2) is no longer accurate. Therefore, the characteristics of ZVS quasi-resonant LED drivers for small L need to be derived.

A 22-W ZVS quasi-resonant LED driver was presented in [14]. The LED driver operates at a fixed switching frequency of 11 MHz with a 67 kHz envelope, and the LED current is controlled by adjusting the ON time of the envelope. However, ZVS might not be achieved under different voltages and current conditions with a fixed-duty-ratio fixed-frequency signal. Since ZVS is the key to maintain high power efficiency with high switching frequency, the conditions for quasi-resonant LED drivers to achieve ZVS need to be analyzed in detail, and the corresponding control method should always ensure ZVS.

A ZVS quasi-resonant LED driver, however, brings several challenges to the power switch. The high switching frequency requires a fast switching speed, which means small parasitic capacitance. Meanwhile, to achieve a high power efficiency in high-voltage applications, the on-resistance–drain–capacitance

product $R_{ON} \times C_d$ needs to be small. Finally, the voltage stress on the power switch requires a high breakdown voltage. gallium nitride (GaN) devices have demonstrated excellent performance for highly efficient power switching applications due to the superior material properties [15], [16]. GaN devices can realize high breakdown voltage with a low R_{ON} due to the large critical electric field and the high density 2-D electron gas with high carrier mobility. GaN devices also show small gate and drain capacitance compared to their Si counterparts because of the lateral device structure. Therefore, a GaN device is a more suitable choice for the power switch of a ZVS quasi-resonant LED driver than a Si MOSFET.

LEDs are usually connected in series to ensure a uniform current. However, as LEDs age, some of them may fail and cause an open circuit, resulting in the failure of the whole LED string. The lifetime of the LED string is therefore determined by the worst LED. Applications such as streetlights and factory lighting require high reliability and long lifetime of LED strings to reduce the maintenance cost. To achieve this goal, an LED open-failure protector that bypasses failed LEDs can be used. In [17] and [18], the bypass circuits consist of 3–5 off-chip components including a zener diode, a silicon-controlled rectifier (SCR), capacitors, and resistors, which are bulky solutions. [19] and [20] proposed LED open-failure bypass circuits in one device. However, since they are not integrated with the LED driver, the complexity and cost of the LED system is increased. Besides these drawbacks, all the above mentioned LED open-failure bypass circuits use an SCR. If the operating current of the LED is lower than the holding current of the SCR, these LED open-failure bypass circuits will not be able to function properly.

Motivated by the above concerns, an auto-ZVS quasi-resonant LED driver with GaN FETs and fully integrated LED shunt protectors (LEDSPs) is presented. This paper is organized as follows. Section II discusses the characteristics of ZVS quasi-resonant LED drivers with small inductors, including the steady-state operation principles and the conditions for ZVS. The proposed LED driver is introduced in Section III. The guidelines for components selection are presented in Section IV. Measurement results are shown in Section V. Finally, conclusions are drawn in Section VI.

II. CHARACTERISTICS OF ZVS QUASI-RESONANT LED DRIVERS

A. Topology and Steady-State Operating Principles

Fig. 1(b) shows the more accurate steady-state operation principles of a ZVS quasi-resonant LED driver [21]. In this analysis, L is treated as a real inductor instead of being simplified as a constant current source. A switching cycle can be divided into four stages.

At $t = 0$, the power switch has just turned off, and the diode is also off. L has just finished its charging phase, and the current going through L is at its peak value I_{Lpeak} . In stage 1 ($0 < t < t_1$), V_x ramps up until it reaches V_{IN} . Since t_1 is very short, i_{LR} will not change much and C_d is approximately linearly charged by I_{Lpeak} . In stage 2 ($t_1 < t < t_2$), when V_x reaches V_{IN} , the diode will be turned on. L is linearly

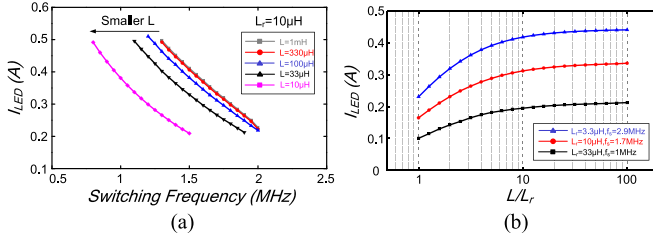


Fig. 2. Simulation results of I_{LED} of a ZVS quasi-resonant LED driver. Number of LEDs = 20, $V_{IN} = 100$ V, $L_r = 10 \mu\text{H}$, and $C_d = 60 \text{ pF}$. (a) I_{LED} versus f_s . (b) I_{LED} versus L/L_r .

discharged and L_r resonates with C_d until V_D reaches zero voltage (ZV). In stage 3 ($t_2 < t < t_3$), after V_D reaches ZV, it will be clamped by the body diode of Q, which will conduct the reverse current, and V_D will remain 0 V. L_r is linearly charged, while L is linearly discharged in this stage until i_{Lr} crosses i_L . In stage 4 ($t_3 < t < T$), after i_{Lr} crosses i_L , the diode is forced to turn off. L_r and L are linearly charged until Q is turned off again.

According to this analysis, whose detailed procedure can be found in [21], the conversion ratio of the ZVS quasi-resonant LED driver can be obtained as

$$\begin{aligned} M &= \frac{V_{LED}}{V_{IN}} \\ &= 1 - \frac{f_s}{2\pi f_r} \left[(1-M)(\alpha' + \beta') + \frac{1 + \sqrt{1 - \beta'^2 + \alpha'^2}}{\beta'} \right. \\ &\quad \left. + \arcsin \frac{\beta'}{\sqrt{1 + \alpha'^2}} - \arctan \alpha' + \pi \right] \end{aligned} \quad (4)$$

where

$$\begin{aligned} \beta' &= \frac{V_{IN}}{I_{L\text{peak}}} \sqrt{\frac{C_d}{L_r}}, \quad \alpha' = \frac{L_r}{L} M \beta' \\ I_{L\text{peak}} &= I_{LED} + \frac{\pi V_{LED} \sqrt{C_d L_r}}{L + M L_r}. \end{aligned} \quad (5)$$

For a standard buck converter, the voltage conversion ratio equals the duty ratio of the gate voltage of Q. Accordingly, the output of a buck converter is usually controlled by modulating the duty ratio while keeping the switching frequency fixed. However, the switching frequency instead of the duty ratio appears on the right-hand side of (4). Therefore, the output of the ZVS quasi-resonant LED driver should be controlled by the switching frequency.

Compared with (2), another factor α' , which is reversely proportional to L , is introduced into (4). In addition, β' depends on $I_{L\text{peak}}$ instead of I_{LED} . When L is very large, the current ripple going through L is very small. α' is close to 0 and β' almost equals β , which makes (2) and (4) very close to each other. However, if a small L is used, the current ripple going through L will be large. β' will be considerably smaller than β , and α' cannot be neglected anymore. Under such circumstances, (4) is more accurate to describe the steady-state characteristics of the ZVS quasi-resonant LED driver.

Fig. 2(a) shows the simulation results of the LED current of the ZVS quasi-resonant LED driver with L_r of $10 \mu\text{H}$.

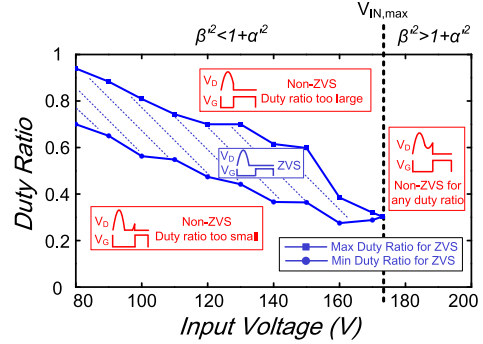


Fig. 3. Conditions for ZVS.

As the switching frequency increases, the current of the LEDs decreases. When L is relative large, the characteristics of the ZVS quasi-resonant LED driver is barely affected by the value of L . As L becomes smaller, its value affects the characteristics of the ZVS quasi-resonant LED driver more significantly. Fig. 2(b) shows the simulation results with different values of L_r . With the same switching frequency, the current of the LEDs starts to change significantly when L/L_r is smaller than 10. Therefore, $L/L_r = 10$ can be used as the boundary between a large L and small L as a rule of thumb.

B. Conditions for ZVS

Mathematically, if $V_D = 0$ has real solutions, ZVS can be achieved. Therefore, the first condition for ZVS is that

$$V_D = V_{IN} + \frac{\sqrt{1 + \alpha'^2}}{\beta'} V_{IN} \sin(\omega_r(t - t_1) + \arctan \alpha'). \quad (6)$$

In stage 2 ($t_1 < t < t_2$), L_r resonates with C_d . To achieve ZVS, the magnitude of resonance should be large enough such that the valley of V_D is able to touch 0 V. According to [21], V_D can be expressed as

$$\beta'^2 < 1 + \alpha'^2. \quad (7)$$

Whether ZVS can be achieved is also determined by the timing of turning on Q. Before t_2 , V_D is larger than 0 V. After i_{Lr} crosses 0 A and becomes positive again, if Q is still not turned on, its power diode will stop conducting reverse current. Then, C_d will be charged again, and V_D will rise from 0 V. Therefore, Q should be turned on after t_2 , and before i_{Lr} rises to cross 0 A. In other words, the duty ratio of the gate voltage of Q should be within a certain range. The second condition for ZVS is that

$$1 - t_{(i_{Lr}=0)} f_s < D < 1 - t_2 f_s. \quad (8)$$

Fig. 3 shows the simulation results of conditions for ZVS. Twenty LEDs are driven at 350 mA with $L = L_r = 3.3 \mu\text{H}$ and $C_d = 60 \text{ pF}$. There is a maximum input voltage $V_{IN,\text{max}}$ for ZVS, which is determined by (7). When the input voltage is larger than $V_{IN,\text{max}}$, the valley of V_D is larger than 0 V and ZVS cannot be achieved with any duty ratio. When the input voltage is smaller than $V_{IN,\text{max}}$, ZVS can be achieved within a window of the duty ratio. As the input voltage increases, both the maximum and minimum duty ratio for ZVS decreases.

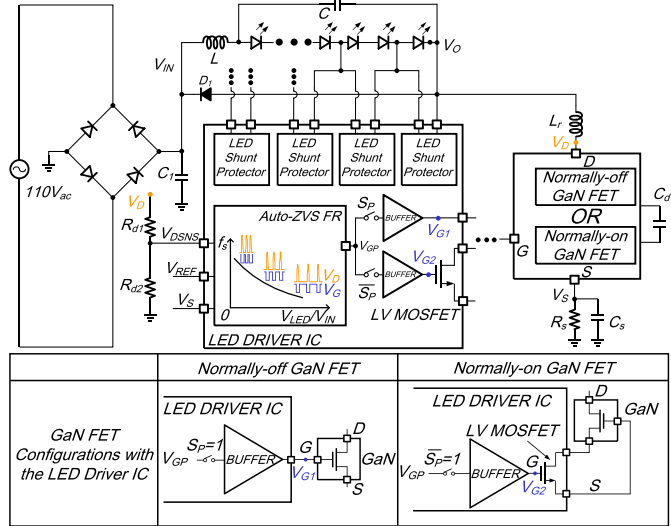


Fig. 4. System architecture of the proposed LED driver.

If a fixed duty ratio is used, the quasi-resonant LED driver will not be able to achieve ZVS in the whole range of input voltage. Therefore, the duty ratio of the gate driving voltage V_G should be adjustable for different voltages and LED currents.

III. PROPOSED LED DRIVER SYSTEM

A. System Architecture

The system architecture of the proposed auto-ZVS quasi-resonant LED driver with a GaN FET and fully integrated LEDSPs is shown in Fig. 4. The GaN FET is used as the power switch. Its fast speed enables high switching frequency operation, and with its superior $R_{ON} \times C_d$, the power efficiency of the proposed LED driver can be improved significantly. With different connections to the GaN FET, the proposed LED driver is able to use either a normally ON or a normally OFF GaN FET. R_S and C_S sense the current and feed it back to the auto-ZVS frequency regulator (FR), which controls the LED current and makes sure ZVS is always achieved, to maintain a high efficiency. During the OFF time of the GaN FET, L_r resonates with C_d , which makes V_D drop to ZV before the GaN FET is turned on to achieve ZVS. If V_D is not ZV before the GaN FET turns on, the auto-ZVS FR will adaptively adjust the duty ratio of V_G to ensure ZVS. Instead of using an off-chip LED open-failure bypass circuit, four LEDSPs are fully integrated with the LED driver circuit. One LEDSP can be connected in parallel with one or multiple LEDs to monitor their status and provide current bypass if these LEDs fail. The lifetime of the LED string can be improved, and the maintenance cost can be reduced with a high level of system integration.

B. Auto-ZVS FR

Fig. 5(a) shows the implementation of the auto-ZVS FR. The control loop mainly consists of an error amplifier (EA) and a voltage-controlled oscillator (VCO). The EA provides a high gain for the control loop such that V_S will be forced to equal V_{REF} , and the VCO provides the gate voltage of

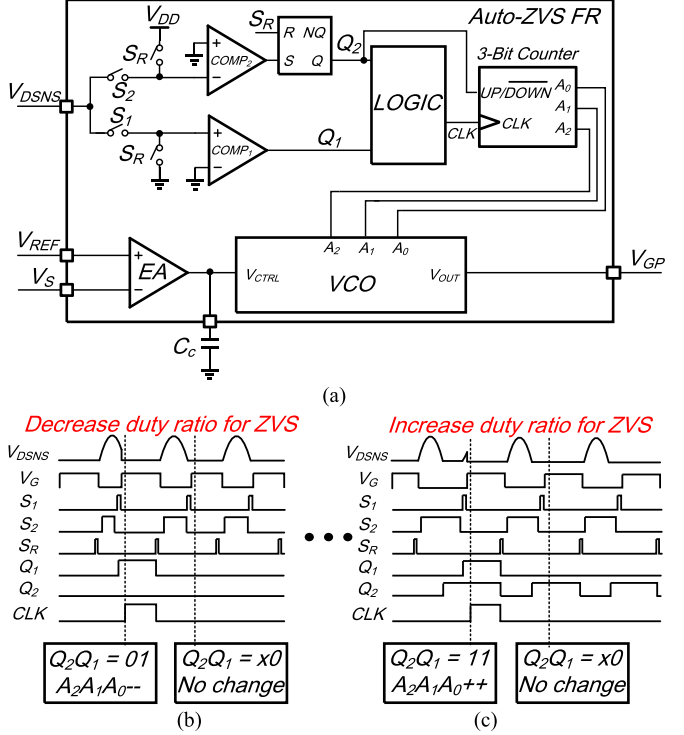


Fig. 5. (a) Implementation of the auto-ZVS FR. (b) Situation of decreasing duty ratio for ZVS. (c) Situation of increasing duty ratio for ZVS.

the GaN FET with different switching frequencies and duty ratios. During steady state, V_S equals V_{REF} . If I_{LED} suddenly increases, V_S will rise and become larger than V_{REF} . The output of the EA will drop, and the switching frequency produced by the VCO will increase. With larger switching frequency, I_{LED} will drop until V_S equals V_{REF} again. In this way, the LED current is regulated. A capacitor C_C is connected at output of the EA to achieve dominant pole compensation.

To ensure ZVS is achieved under different conditions, the duty ratio of the VCO can be automatically adjusted. As $A_2A_1A_0$ increases from 000 to 111, the duty ratio increases from about 0.2 to about 0.8. Two comparators, four switches, and an RS latch are used to translate the sensed drain voltage (V_{DSNS}) into a digital signal for the logic circuits to process. If non-ZVS is sensed, the logic circuits will send a pulse signal (CLK) to the 3-bit bidirectional counter to adjust the duty ratio, and the output of the RS latch, namely, Q_2 , determines whether the duty ratio should be increased or decreased. Fig. 5(b) and (c) shows the key waveforms of the auto-ZVS FR. S_1 is used to sample V_{DSNS} just before V_G is high. S_2 is used to monitor V_{DSNS} during the OFF time of V_G , and S_R is used to reset the comparator at the end of each cycle. If V_{DSNS} fails to drop to ZV before the GaN FET is turned on, non-ZVS appears and the output of $COMP_1$, namely, Q_1 , will be 1. The two situations of non-ZVS are shown in Fig. 5(b) and (c), respectively. The values of Q_2Q_1 will be checked shortly after V_G is on to determine the duty ratio. If V_{DSNS} has not reached ZV during the OFF time of V_G , $Q_2Q_1 = 01$. In this case, the 3-bit counter will count down by 1 and duty ratio will be decreased to achieve ZVS, as shown in Fig. 5(a). On the other hand, if V_{DSNS} has reached ZV

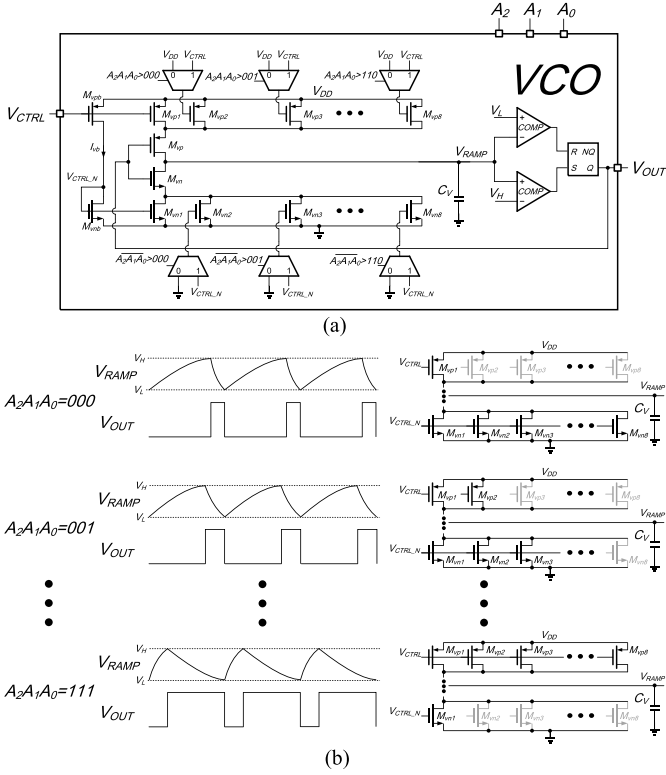


Fig. 6. (a) Implementation of the VCO. (b) Waveforms and equivalent circuits of VCO with different duty ratios.

during the OFF time of \$V_G\$, \$Q_2Q_1 = 11\$, and the duty ratio will be increased, as shown in Fig. 5(b). \$Q_2Q_1 = x0\$ means ZVS has already been achieved, and the duty ratio will remain the same.

C. VCO

Fig. 6(a) shows the circuit implementation of the VCO. \$M_{vp1}\$–\$M_{vp8}\$ and \$M_{vn1}\$–\$M_{vn8}\$ controls the charging and discharging current of \$C_V\$, respectively. \$V_{RAMP}\$ is bounded by \$V_H\$ and \$V_L\$. When \$V_{RAMP}\$ hits \$V_H\$ or \$V_L\$, the RS latch will be set or reset to discharge or charge \$C_V\$, respectively. \$V_{CTRL}\$ controls the switching frequency of the VCO by controlling the charging and discharging current of \$C_V\$.

The duty ratio of the VCO is controlled by changing the number of charging and discharging transistors. Of \$M_{vp1}\$–\$M_{vp8}\$ and \$M_{vn1}\$–\$M_{vn8}\$, a total of nine transistors are used to charge and discharge \$C_V\$. As shown in Fig. 6(b), when \$A_2A_1A_0 = 000\$, \$M_{vp1}\$ and \$M_{vn1}\$–\$M_{vn8}\$ will be active. The charging current of \$C_V\$ is much smaller than the discharging current, resulting in a very small duty ratio. As \$A_2A_1A_0\$ counts up by 1, the number of the charging PMOS will increase by 1 and the number of the discharging NMOS will decrease by 1. The duty ratio will therefore be larger. When \$A_2A_1A_0 = 111\$, \$M_{vp1}\$–\$M_{vp8}\$ and \$M_{vn1}\$ will be active. The charging current of \$C_V\$ is much larger than the discharging current. Under this condition, the VCO has maximum duty ratio. Eight levels of duty ratio can be achieved. The sizes of the transistor are designed as

$$\left(\frac{W}{L}\right)_{M_{vp1}} : \left(\frac{W}{L}\right)_{M_{vp2-8}} = \left(\frac{W}{L}\right)_{M_{vn1}} : \left(\frac{W}{L}\right)_{M_{vn2-8}} = 2. \quad (9)$$

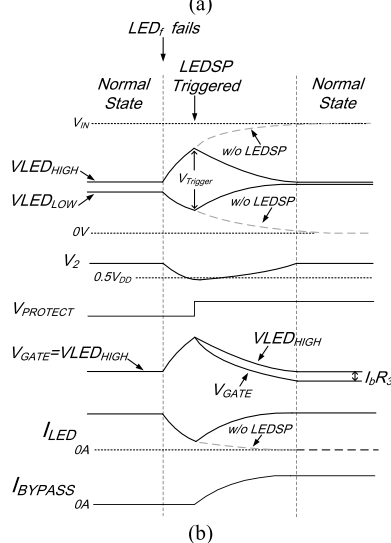
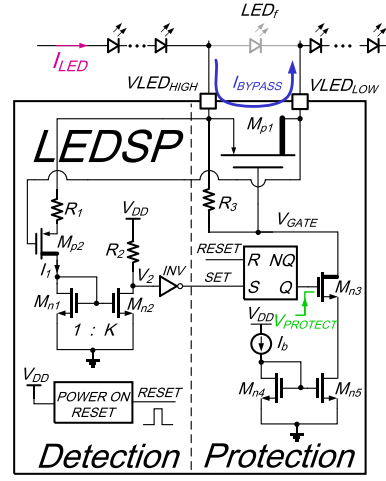


Fig. 7. (a) Implementation of the LEDSP. (b) Waveforms of the LEDSP.

The designed maximum and minimum duty ratio are 0.812 and 0.182, respectively, and the step size of the duty ratio is 0.091.

D. Fully Integrated LED Shunt Protector

Fig. 7(a) and (b) shows the implementation of the fully integrated LEDSP and its key waveforms, respectively. The status of the LEDs is monitored by the left half of the LEDSP. When all the LEDs are working properly, \$V_{LEDHIGH} - V_{LEDDLOW}\$ equals the forward voltage of the LEDs connected to the LEDSP. \$I_1\$ is small, and \$V_2\$ is above the threshold voltage of the inverter. \$M_{n3}\$ is OFF, and the gate-source voltage of the power transistor \$M_{p1}\$ equals 0 V. There is no current going through the LEDSP. If LED_f fails and causes an open circuit, \$V_{LEDHIGH}\$ will rise toward \$V_{IN}\$ and \$V_{LEDDLOW}\$ will drop toward ground. The rising of \$V_{LEDHIGH} - V_{LEDDLOW}\$ makes \$I_1\$ increase and \$V_2\$ decrease. When \$V_{LEDHIGH} - V_{LEDDLOW}\$ surpasses the designed trigger voltage, \$V_{PROTECT}\$ will rise from low to high, turning on \$M_{n3}\$ to allow mirrored \$I_b\$ to flow through \$R_3\$. As a result, the power on reset circuit generates a pulse signal to reset the RS latch every time the system is rebooted.

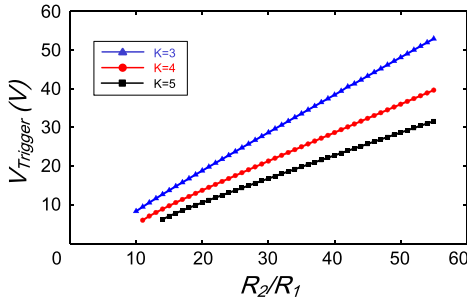


Fig. 8. Simulation results of trigger voltage of the LEDSP.

In this way, the LEDSP can be put into idle state after the failed LEDs are replaced.

The threshold voltage of the inverter is about $0.5 V_{DD}$. The trigger voltage of $(V_{LEDHIGH} - V_{LEDLOW})V_{Trigger}$ can be determined with the following equations:

$$V_{Trigger} = I_1 R_1 + V_{GS,Mp2} = I_1 R_1 + \sqrt{\frac{2I_1}{k_p \left(\frac{W}{L}\right)_{Mp2}}} + V_{thp} \quad (10)$$

$$\frac{1}{2}V_{DD} = K I_1 R_2 \quad (11)$$

where K is the ratio of M_{n2} to M_{n1} . By combining (10) and (11), we have

$$V_{Trigger} = \frac{V_{DD}}{2K} \frac{R_2}{R_1} + \sqrt{\frac{V_{DD}}{KR_2 k_p \left(\frac{W}{L}\right)_{Mp2}}} + V_{thp}. \quad (12)$$

Fig. 8 shows the simulation results of $V_{Trigger}$ with different K and R_2/R_1 . In this design, with $K = 4$ and $R_2/R_1 = 36$, the trigger voltage is about 26 V, and thus one LEDSP can be used to protect one or multiple LEDs.

IV. COMPONENT SELECTION

A. Selection of GaN FET

In stage 2, L_r resonates with C_d , and V_D will rise up to a very high-voltage V_{Dpeak} , as shown in Fig. 1. To stand such high voltage, the breakdown voltage of the GaN FET V_{BR} should be larger than V_{Dpeak}

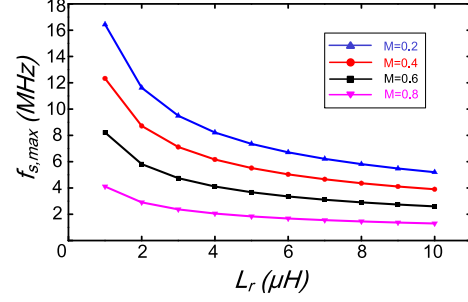
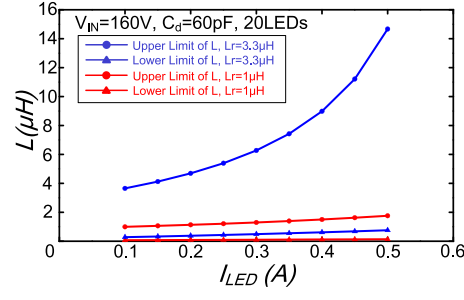
$$V_{Dpeak} = V_{IN} \left(1 + \frac{\sqrt{1 + \alpha'^2}}{\beta'} \right) < V_{BR}. \quad (13)$$

According to (6), V_{Dpeak} is larger than $2V_{IN}$. Usually, the GaN FET is selected with a V_{BR} of at least 3–4 times V_{IN} . For example, for an 110 V_{ac} design, V_{BR} should be at least 600 V.

B. Selection of L_r

L_r is the key component to determine the maximum switching frequency of the ZVS quasi-resonant LED driver. The switching frequency reaches its maximum value when $\beta' = (1 + \alpha'^2)^{1/2}$. Combined with (4), the approximate maximum switching frequency can be obtained as

$$f_{s,\max} \approx (1 - M) f_r. \quad (14)$$

Fig. 9. Maximum switching frequency with different L_r .Fig. 10. Range of L . $V_{IN} = 160$ V, $C_d = 60$ pF, and number of LEDs = 20.

The maximum switching frequency is determined by the resonant frequency f_r , which is a function of C_d and L_r according to (3). As C_d is the parasitic drain capacitance of the GaN FET and cannot be changed once the GaN FET is selected, the value of L_r can be obtained as

$$L_r = \frac{(1 - M)^2}{(2\pi f_{s,\max})^2 C_d}. \quad (15)$$

Fig. 9 shows the maximum switching frequency with different L_r and M . With a smaller L_r , the ZVS quasi-resonant LED driver will operate at a higher range of switching frequency.

C. Selection of L

As L becomes smaller, the current ripple of L and L_r , and the magnitude of resonance of V_D becomes larger. ZVS will be easier to achieve. However, the peak voltage V_{Dpeak} , which should not exceed V_{BR} , will also be larger with a smaller L . Therefore, the value of L should meet both the requirements of ZVS and breakdown voltage of the GaN FET.

By combining (7) and (13), the range of β' can be obtained. Since $(1 + \alpha'^2)^{1/2}$ is always close to 1, the range of β' can be rewritten as

$$\frac{V_{IN}}{V_{BR} - V_{IN}} < \beta' < 1. \quad (16)$$

Substituting (5) into (16), the range of L can be obtained as

$$\frac{\pi V_{LED} \sqrt{C_d L_r}}{(V_{BR} - V_{IN}) \sqrt{\frac{C_d}{L_r}} - I_{LED}} - M L_r < L < \frac{\pi V_{LED} \sqrt{C_d L_r}}{V_{IN} \sqrt{\frac{C_d}{L_r}} - I_{LED}} - M L_r. \quad (17)$$

The upper limit of L is set by the conditions for ZVS, and the lower limit of L is set by V_{BR} . Fig. 10 shows an example

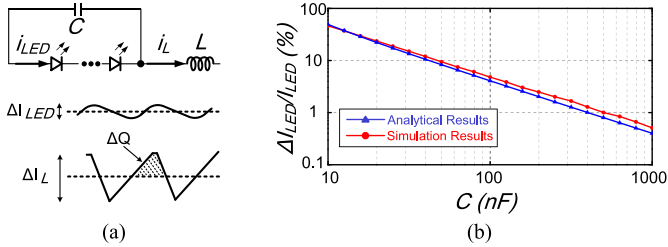


Fig. 11. (a) Current ripple of the LEDs. (b) Simulation and analytical results of the current ripple of the LEDs with different C . $N = 20$, $I_{LED} = 500$ mA, $V_{IN} = 160$ V, $L = L_r = 3.3$ μ H, and $C_d = 60$ pF.

of the range of L with different L_r and I_{LED} . As L_r or I_{LED} increases, the range of L becomes wider.

D. Selection of C

When a small L is used, the current ripple going through L is very large. In some cases, i_L can even be negative. To filter the current ripple, a capacitor C in parallel with the LEDs is needed. A capacitor that is too small will not be able to reduce the current ripple of the LEDs. A large C can ensure small current ripple. However, high-voltage capacitors of large values are usually bulky and expensive. Therefore, the value of C needs to be carefully chosen to meet the requirements at minimum cost. As shown in Fig. 11(a), the voltage ripple of the LED can be expressed as

$$\Delta V_{LED} = \frac{\Delta Q}{C} = \frac{\frac{1}{2} \times \frac{1}{2} T \times \frac{1}{2} \Delta I_L}{C} = \frac{(1-M)V_{LED}}{8(L+ML_r)f_s^2C}. \quad (18)$$

Since the LEDs are essentially diodes, the current ripple of the LEDs is

$$\begin{aligned} \Delta I_{LED} &= i_s \left(e^{\frac{V_{LED} + \Delta V_{LED}}{nNVT}} - 1 \right) - i_s \left(e^{\frac{V_{LED}}{nNVT}} - 1 \right) \\ &= I_{LED} \left(e^{\frac{\Delta V_{LED}}{nNVT}} - 1 \right) \end{aligned} \quad (19)$$

where N is the number of the LEDs and n is the emission coefficient of one LED. Combining (18) and (19), the value of C can be determined by

$$C = \frac{(1-M)V_{LED}}{8(L+ML_r)f_s^2NnVT \ln(1 + \frac{\Delta I_{LED}}{I_{LED}})}. \quad (20)$$

Fig. 11(b) shows an example of the simulation results and analytical results of LED current ripple with different C . The LED current ripple can be reduced to less than 10% with a C of 100 nF.

E. Power Efficiency Considerations

L , L_r , and the GaN FET are the top three most power consuming components in the proposed LED driver. Selection of these components also affects the power efficiency. As shown in Fig. 1(b), i_L can be broken down into a dc part and an ac part, while i_{Lr} has a much larger ac part than

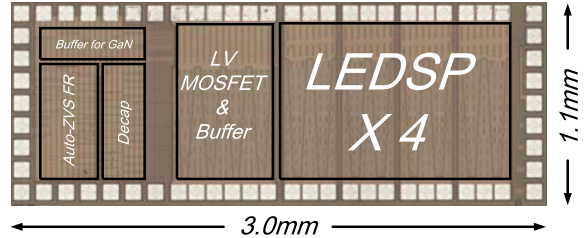


Fig. 12. Chip micrograph of the proposed driver IC.

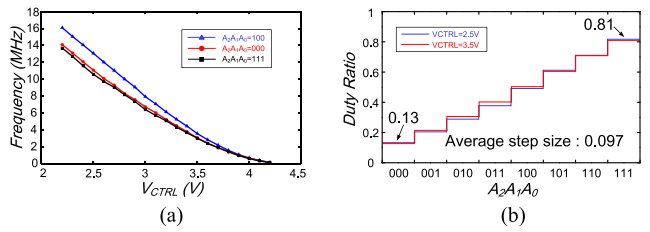


Fig. 13. Measurement results of the VCO. (a) Frequency versus control voltage. (b) Duty ratio versus $A_2A_1A_0$.

dc part. By combining (5), the power loss on L , L_r , and the GaN FET can be estimated as

$$\left\{ \begin{array}{l} P_{loss,L} = \frac{1}{2} I_{LED}^2 R_L + \frac{1}{3} \frac{\pi^2 V_{LED}^2 C_d}{\left(\frac{L}{\sqrt{L_r}} + M\sqrt{L_r} \right)^2} R_L \\ P_{loss,Lr} = k_1 I_{LPeak}^2 R_{Lr} = k_1 \frac{\pi^2 V_{LED}^2 C_d}{\left(\frac{L}{\sqrt{L_r}} + M\sqrt{L_r} \right)^2} R_{Lr} \\ P_{loss,GaN} = k_2 I_{LPeak}^2 R_{ON} = k_2 \frac{\pi^2 V_{LED}^2}{\left(\frac{L}{\sqrt{L_r}} + M\sqrt{L_r} \right)^2} C_d R_{ON} \end{array} \right. \quad (21)$$

where R_L and R_{Lr} are the parasitic resistance of L and L_r , respectively, R_{ON} is the on-resistance of the GaN FET, and k_1 and k_2 are constants between 0 and 1. According to (21), for the GaN FET, the $R_{ON} \times C_d$ should be as small as possible to minimize its power loss. For the inductors, designers should select those with small parasitic resistance. Besides that the inductance also affects the power efficiency. As L increases, the current ripple decreases and results in less power loss. L_r is not a crucial factor to the power efficiency and is usually selected to meet the requirement of frequency range.

V. MEASUREMENT RESULTS

The proposed driver IC was fabricated with a 0.35- μ m 120-V high-voltage CMOS process, and the micrograph of the die is shown in Fig. 12. The chip measures 3 mm \times 1.1 mm, and includes an auto-ZVS FR, a buffer for a normally OFF GaN FET, a low-voltage (LV) MOSFET for a normally ON GaN FET, and four LEDSPs. The supply voltage for the controller is 5.5 V.

The measurement results of the VCO are shown in Fig. 13. The VCO is designed to mainly operate at MHz range, which is also the frequency range of the proposed LED driver. The output frequency of the VCO decreases from 16.1 MHz to 188 kHz as the control voltage increases from 2.2 to 4.2 V when $A_2A_1A_0 = 100$. The duty ratio of the VCO increases

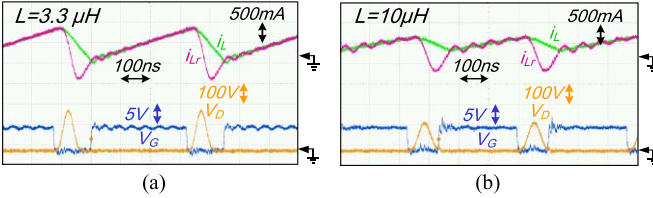


Fig. 14. Measured waveforms of V_D , V_G , i_L , and i_{LR} with different L . $V_{IN} = 100$ V, number of LEDs = 10, and $L_r = 3.3 \mu\text{H}$. (a) $L = 3.3 \mu\text{H}$. (b) $L = 10 \mu\text{H}$.

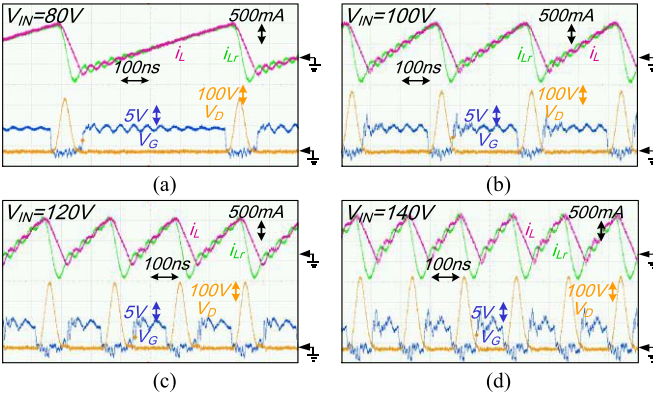


Fig. 15. Measured waveforms of V_D , V_G , i_L , and i_{LR} with different input voltages. Number of LEDs = 20, $L_r = 3.3 \mu\text{H}$, and $L = 3.3 \mu\text{H}$. (a) $V_{IN} = 80$ V. (b) $V_{IN} = 100$ V. (c) $V_{IN} = 120$ V. (d) $V_{IN} = 140$ V.

as $A_2A_1A_0$ counts up. The measured maximum and minimum duty ratios are 0.81 and 0.13, respectively. The average step size is about 0.097.

Fig. 14 shows the measured waveforms of V_D , V_G , i_L , and i_{LR} with different L . Ten 1-W LEDs are driven under 100-V_{dc} input with L_r of 3.3 μH and L of 3.3 and 10 μH . A commercial normally OFF GaN FET [22] is used as the power switch. The waveforms match the analytical results shown in Fig. 1(b). With a smaller L , ZVS is easier to achieve with the sacrifice of larger current ripple and peak voltage.

Fig. 15 shows the measured waveforms of V_D , V_G , i_L , and i_{LR} under different dc input voltages. The proposed LED driver powers 20 1-W LEDs with $L = L_r = 3.3 \mu\text{H}$. As the input voltage increases from 80 to 140 V_{dc}, the switching frequency is increased by the auto-ZVS FR from 1.70 to 5.7 MHz. To ensure ZVS operation, the duty ratio is decreased from 80% to 50%.

Fig. 16 shows the measurement results of the proposed LED driver with a normally OFF GaN FET under 60-Hz 100- to 120-V_{ac} input. Twenty 1-W LEDs in parallel with capacitor of 330 nF are driven with $L = L_r = 3.3 \mu\text{H}$. Situations of increasing duty ratio for ZVS and decreasing duty ratio for ZVS are shown in the top right and bottom right of Fig. 16(a), respectively.

Due to the existence of 2-D electron gas, GaN FETs are usually of the normally ON type. To demonstrate the functionality of the proposed LED driver, a normally ON GaN FET is designed and fabricated in the laboratory. Fig. 17 shows the chip photograph of the in-house-fabricated GaN FET and its connection with the proposed LED driver. The normally ON GaN FET needs to be cascaded with an on-chip LV MOSFET,

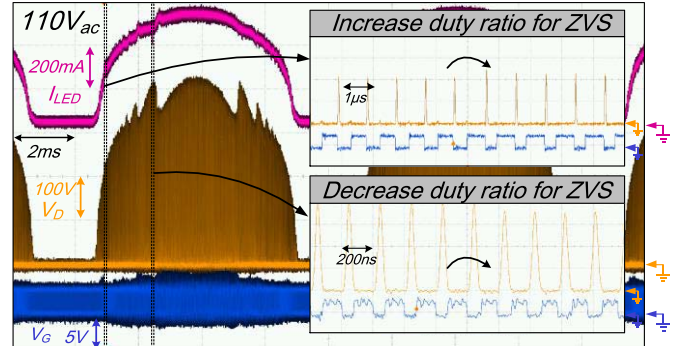


Fig. 16. Measured waveforms of the proposed LED driver with a normally OFF GaN FET under 60-Hz 100- to 120-V_{ac} input. Number of LEDs = 20 and $L = L_r = 3.3 \mu\text{H}$. (a) 110 V_{ac} . (b) 100 V_{ac} . (c) 120 V_{ac} .

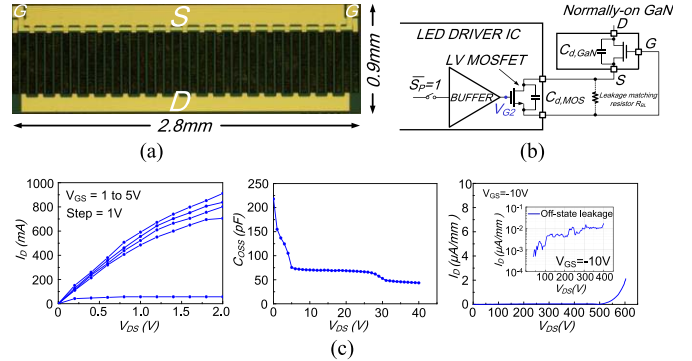


Fig. 17. (a) Chip micrograph of the in-house-fabricated normally ON GaN FET. (b) Connection between the LED driver IC and the normally ON GaN FET. (c) Measured output characteristics and C_{oss} of the normally ON GaN FET cascoded with the LV MOSFET and the OFF-state leakage of the normally ON GaN FET.

and V_{G2} is connected to the gate of the LV MOSFET. When V_{G2} is high, the GaN FET is turned on by the nearly zero V_{SD} of the MOSFET, and when V_{G2} is low, the GaN FET is turned off by the negative V_{SD} of the MOSFET.

The drain capacitor of the normally ON GaN FET and the MOSFET is connected in series, and the $C_{d,GaN}$ is small compared with $C_{d,MOS}$, making the total drain capacitance of the cascaded power switch dominated by $C_{d,GaN}$. The $R_{ON} \times C_d$ of the cascaded power switch is determined by $C_{d,GaN} \times (R_{ON,GaN} + R_{ON,MOS})$. Therefore, to minimize the power loss, the size of the LV MOSFET should be designed relatively large. The leakage current of the GaN FET is usually much larger than that of the MOSFET. During the OFF-state of the cascaded power switch, the source of the GaN FET may rise to a very high voltage due to the leakage mismatch and damage the LV MOSFET. To prevent this from happening, a leakage matching resistor R_{BL} of 10 M Ω is connected in parallel with the LV MOSFET, as shown in Fig. 17(b).

TABLE I
PERFORMANCE COMPARISON WITH PREVIOUS WORK

	[5]	[8]	[13]	[14]	[23]	This Work
Process	0.35- μ m BCDMOS	0.35- μ m 120-V HVCmos	0.35- μ m 700-V BCMOS	0.5- μ m 500-V LDMOS	0.5- μ m 500-V BCDMOS	0.35-μm 120-V HVCmos
Off-Chip Power Switch	800-V MOSFET	No	No	600-V GaN FET & LV MOSFET	No	600-V GaN FET
Magnetics	Transformer 1.8 mH	Inductor 10–39 μ H	Inductors 3.9 μ H \times 2	Inductors 850 nH & 12 μ H	Inductor 5.5 mH	Inductors 3.3 μH \times 2
HV Capacitor	Electrolytic 470 μ F	MLCC 220 nF	MLCC 1 μ F	MLCC 15 μ F	MLCC 1 μ F	MLCC 330 nF \times 2
Output Power	6–12 W	1–25 W	16–28 W	7–22 W	2.5–7 W	20–25 W
Input Voltage	180–260 V _{ac}	115 V _{dc}	120 V _{dc}	100–120 V _{ac}	50–320 V _{ac}	100–120 V_{ac}
LED Protection	No	No	No	No	No	Fully Integrated
Power Factor	0.96	N. A.	N. A.	0.96	0.98/0.92	0.973
Peak Efficiency	85%	88% @ 115 V _{dc}	84% @ 120 V _{dc}	90.6%	89%	91.4%
Flicker	<5%	N.A.	N.A.	100%	100%	100%

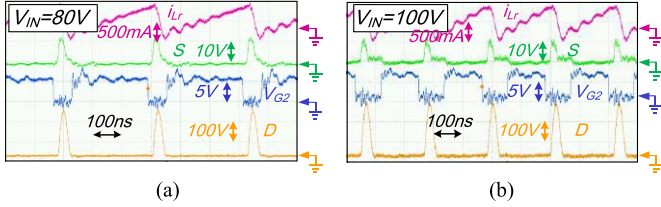


Fig. 18. Measured waveforms of the proposed LED driver with a normally ON GaN FET under (a) 80 V_{dc} and (b) 100 V_{dc}.

Fig. 17(c) shows the measured output characteristics and C_{oss} of the cascaded power switch and the OFF-state leakage of the normally ON GaN FET. Fig. 18 demonstrates the functionality of the proposed LED driver with the normally ON GaN FET under 80- to 100-V_{dc} input.

The testing setup of the trigger voltage of the LEDSP is shown in Fig. 19(a). R_{a1} and R_{a2} are connected in series with a voltage source V_{test} , which is gradually increased from 0 V. When V_{test} is smaller than $V_{Trigger}$, the LEDSP is not triggered and most of the voltage drops on R_{a1} . As V_{test} surpasses $V_{Trigger}$, the power transistor in the LEDSP is turned on and most of the voltage will drop on R_{a2} . The measurement results are shown in Fig. 19(b), where $V_{Trigger}$ is 26.5 V and the gate-source voltage of the power transistor in the triggered LEDSP is about -5.1 V. Fig. 20 shows the measurement of the LEDSP in the situation where an LED suddenly fails. A string of 20 LEDs is driven by the proposed LED driver under 110 V_{ac} input. A failed LED is connected in parallel with a functioning LED and the LEDSP. When the switch S_f is on, all the LEDs are working properly and no current is going through the LEDSP. Then, S_f is turned off to simulate the situation where an LED suddenly fails. As S_f is off, I_{LED} begins to drop and the voltage across the LEDSP begins to rise. The LEDSP is then triggered and the current starts to

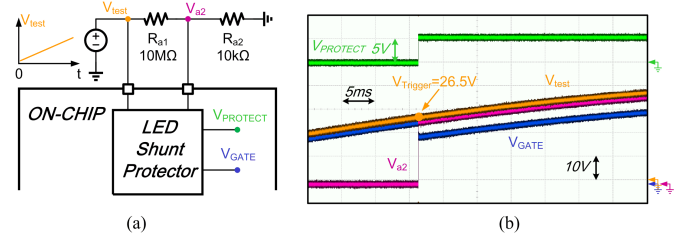


Fig. 19. Measurement of the trigger voltage of the LEDSP. (a) Testing setup. (b) Measurement results.

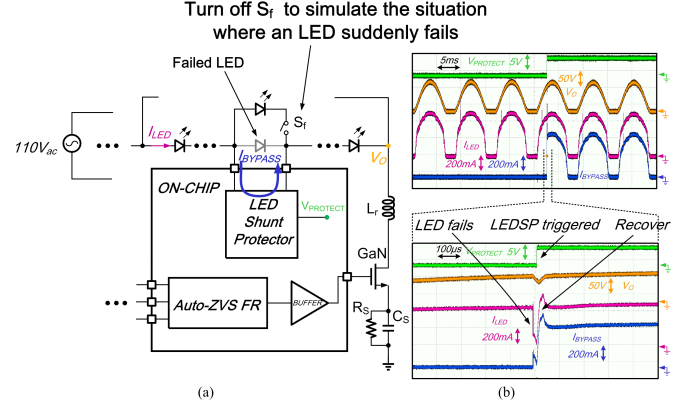


Fig. 20. Measurement of the LEDSP when an LED suddenly fails. (a) Testing setup. (b) Measurement results.

flowthrough the LEDSP, putting the LED string back to work in less than 50 μ s, as shown in Fig. 20(b).

Fig. 21 shows the measured performance of the proposed LED driver under 60-Hz 100- to 120-V_{ac} input. The LED driver drives 20–25 1-W LEDs with $L = L_r = 3.3 \mu$ H and a normally OFF GaN FET. The measured peak efficiency is 91.4%. The power loss caused by the GaN FET, L , L_r ,

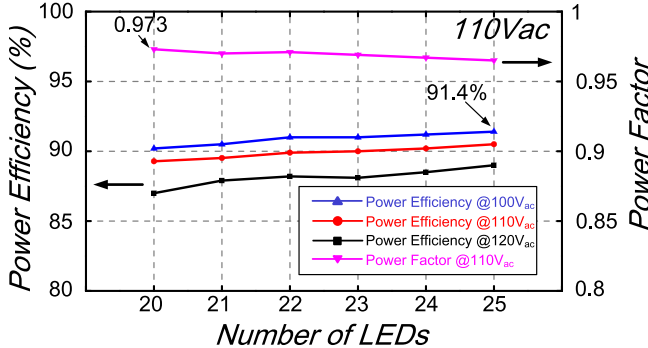


Fig. 21. Measured performance of the proposed LED driver with a normally OFF GaN FET and $L = L_r = 3.3 \mu\text{H}$ under 100- to 120-V_{ac} input.

the rectifier bridge, and GaN FET gate driver is about 1.6%, 3%, 3%, 0.6%, and 0.3%, respectively. With an input capacitor of 300 nF to filter the input current ripple, a peak power factor of 0.973 can be achieved. Table I gives a performance comparison with prior art LED drivers. Our design achieves a high power efficiency and power factor with the smallest inductance, and implements fully integrated LED protection.

VI. CONCLUSION

This paper presents an auto-ZVS quasi-resonant LED driver which can drive both normally ON and normally OFF GaN FETs. ZVS can be automatically achieved with the proposed auto-ZVS FR. Four fully integrated LEDSPs are implemented to bypass failed LEDs and improve the lifetime of the LED string. The design is fabricated with a 0.35- μm 120-V high-voltage process. The LED driver can provide up to 25-W power to the LED with $2 \times 3.3 \mu\text{H}$ inductors. Peak efficiency of 91.4% and peak power factor of 0.973 can be achieved with a GaN FET from 60-Hz 100- to 120-V_{ac} input.

REFERENCES

- [1] Y.-K. Cheng and K. W. E. Cheng, "General study for using LED to replace traditional lighting devices," in *Proc. 2nd Int. Conf. Power Electron. Syst. Appl.*, Nov. 2006, pp. 173–177.
- [2] *LM3445 Triac Dimmable Offline LED Driver*, Texas Instrum., Dallas, TX, USA, accessed: Mar. 5, 2013. [Online]. Available: <http://www.ti.com/lit/ds/symlink/lm3445.pdf>
- [3] *LT3799-1 Offline Isolated Flyback LED Controller with Active PFC*, Linear Technol. Corp., Milpitas, CA, USA, accessed: Jun. 12, 2014. [Online]. Available: <http://cds.linear.com/docs/en/datasheet/37991fa.pdf>
- [4] V. Anghel, C. Bartholomeusz, A. G. Vasilica, G. Pristavu, and G. Brezeanu, "Variable off-time control loop for current-mode floating buck converters in LED driving applications," *IEEE J. Solid-State Circuits*, vol. 49, no. 7, pp. 1571–1579, Jul. 2014.
- [5] J. T. Hwang, M. S. Jung, D. H. Kim, J. H. Lee, M. H. Jung, and J. H. Shin, "Off-the-line primary side regulation LED lamp driver with single-stage PFC and TRIAC dimming using LED forward voltage and duty variation tracking control," *IEEE J. Solid-State Circuits*, vol. 47, no. 12, pp. 3081–3094, Dec. 2012.
- [6] K. M. Lau *et al.*, "Cost-effective and eco-friendly LED system-on-a-chip (SoC)," in *Proc. 10th China Int. Forum Solid State Lighting (ChinaSSL)*, Nov. 2013, pp. 235–238.
- [7] R. Wu, J. K. O. Sin, and C. P. Yue, "High-Q backside silicon-embedded inductor for power applications in μH and MHz range," *IEEE Trans. Electron Devices*, vol. 60, no. 1, pp. 339–345, Jan. 2013.
- [8] Z. Liu and H. Lee, "A wide-input-range efficiency-enhanced synchronous integrated LED driver with adaptive resonant timing control," *IEEE J. Solid-State Circuits*, vol. 51, no. 8, pp. 1810–1825, Aug. 2016.

- [9] K.-H. Liu and F. C. Y. Lee, "Zero-voltage switching technique in DC/DC converters," *IEEE Trans. Power Electron.*, vol. 5, no. 3, pp. 293–304, Jul. 1990.
- [10] R. B. Ridley, W. A. Tabisz, F. C. Y. Lee, and V. Vorperian, "Multi-loop control for quasi-resonant converters," *IEEE Trans. Power Electron.*, vol. 6, no. 1, pp. 28–38, Jan. 1991.
- [11] V. Vorperian, R. Tymerksi, and F. C. Y. Lee, "Equivalent circuit models for resonant and PWM switches," *IEEE Trans. Power Electron.*, vol. 4, no. 2, pp. 205–214, Apr. 1989.
- [12] W. A. Tabisz, P. M. Gradzki, and F. C. Y. Lee, "Zero-voltage-switched quasi-resonant buck and flyback converters-experimental results at 10 MHz," *IEEE Trans. Power Electron.*, vol. 4, no. 2, pp. 194–204, Apr. 1989.
- [13] L. Li, Y. Gao, P. K. T. Mok, I. S. M. Sun, and N. Park, "A 16–28-W 92.8%-efficiency monolithic quasi-resonant LED driver with constant-duty-ratio frequency regulator," *IEEE Trans. Circuits Syst. II, Exp. Briefs*, vol. 62, no. 12, pp. 1199–1203, Dec. 2015.
- [14] S. Bandyopadhyay, B. Neidorff, D. Freeman, and A. P. Chandrakasan, "90.6% efficient 11 MHz 22 W LED driver using GaN FETs and burst-mode controller with 0.96 power factor," in *IEEE Int. Solid-State Circuits Conf. (ISSCC) Dig. Tech. Papers*, Feb. 2013, pp. 368–369.
- [15] X. Huang, Z. Liu, Q. Li, and F. C. Lee, "Evaluation and application of 600 V GaN HEMT in cascode structure," *IEEE Trans. Power Electron.*, vol. 29, no. 5, pp. 2453–2461, May 2014.
- [16] M. D. Seeman, S. R. Bahl, D. I. Anderson, and G. A. Shah, "Advantages of GaN in a high-voltage resonant LLC converter," in *Proc. IEEE Appl. Power Electron. Conf. Expo. (APEC)*, Mar. 2014, pp. 476–483.
- [17] C.-C. Chen, C.-Y. Wu, Y.-M. Chen, and T.-F. Wu, "Sequential color LED backlight driving system for LCD panels," *IEEE Trans. Power Electron.*, vol. 22, no. 3, pp. 919–925, May 2007.
- [18] R. Kathiresan, P. Das, T. Reindl, and S. K. Panda, "Novel high-power nonresonant multichannel LED driver," *IEEE Trans. Ind. Electron.*, vol. 64, no. 7, pp. 5851–5864, Jul. 2017.
- [19] *LSP0600BJR Series LED Shunt Protector*, Bourns, Riverside, CA, USA, accessed: Oct. 15, 2015. [Online]. Available: <http://www.bourns.com/docs/Product-Datasheets/LSP.pdf>
- [20] *LBP01 LED Bypass Protection*, STMicroelectronics, Geneva, Switzerland, accessed: Nov. 7, 2015. [Online]. Available: <http://www.st.com/resource/zh/datasheet/lbp01.pdf>
- [21] L. Li, Y. Gao, and P. K. T. Mok, "A more accurate steady state analysis of zero-voltage switching quasi-resonant converters," in *Proc. IEEE Int. Symp. Circuits Syst. (ISCAS)*, May 2016, pp. 1606–1609.
- [22] *TPH3202L 600V Cascode GaN FET PQFN88 Series*, Transphorm, Goleta, CA, USA, accessed: Nov. 12, 2016. [Online]. Available: <http://www.transphormusa.com/document/600v-cascode-gan-fet-tph3202l/>
- [23] J. T. Hwang, K. Cho, D. Kim, M. Jung, G. Cho, and S. Yang, "A simple LED lamp driver IC with intelligent power-factor correction," in *IEEE Int. Solid-State Circuits Conf. (ISSCC) Dig. Tech. Papers*, Feb. 2011, pp. 236–238.



Lisong Li (S'13) received the B.Sc. degree in electronics engineering and computer science from Peking University, Beijing, China, in 2012, and the Ph.D. degree in electronic and computer engineering from The Hong Kong University of Science and Technology, Hong Kong, in 2017.

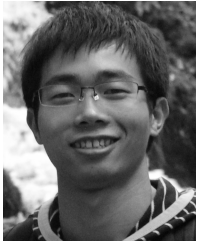
He is currently with CoilEasy Technologies, Shenzhen, China. His current research interests include power management integrated circuit designs and high-voltage LED driver designs.



Yuan Gao (S'13–M'18) received the B.Eng. and M.Eng. degrees from Xi'an Jiaotong University, Xi'an, China, in 2009 and 2012, respectively, and the Ph.D. degree from The Hong Kong University of Science and Technology (HKUST), Hong Kong, in 2017.

He is currently a Post-Doctoral Fellow with HKUST. His current research interests include integrated circuits design for power managements and LED lighting systems.

Dr. Gao was a recipient of the International Solid-State Circuits Conference Student Travel Grant Award in 2017.



Huaxing Jiang (S'13) received the B.S. degree in electronic engineering from Zhejiang University, Hangzhou, China, in 2012, and the Ph.D. degree in electronic and computer engineering from The Hong Kong University of Science and Technology, Hong Kong, in 2017.

He is currently a Post-Doctoral Researcher with The Hong Kong University of Science and Technology. His current research interests include the design and fabrication of GaN-based devices for power and RF applications.



Philip K. T. Mok (S'86–M'95–SM'02–F'14) received the B.A.Sc., M.A.Sc., and Ph.D. degrees in electrical and computer engineering from the University of Toronto, Toronto, ON, Canada, in 1986, 1989, and 1995, respectively.

In 1995, he joined the Department of Electronic and Computer Engineering, The Hong Kong University of Science and Technology, Hong Kong, where he is currently a Professor. His current research interests include semiconductor devices, processing technologies, and circuit designs for power electronics and telecommunications applications, with current emphasis on power management integrated circuits, low-voltage analogue integrated circuits, and RF integrated circuit designs.

Dr. Mok received the Henry G. Acres Medal and the W.S. Wilson Medal from the University of Toronto, and the Teaching Excellence Appreciation Award three times from The Hong Kong University of Science and Technology. He is also a co-recipient of the Best Student Paper Award twice in the 2002 and 2009 IEEE Custom Integrated Circuits Conference. He has been a member of the International Technical Program Committees of the IEEE International Solid-State Circuits Conference from 2005 to 2010 and from 2015 to 2016. He has served as a Distinguished Lecturer for the IEEE Solid-State Circuits Society from 2009 to 2010, and an Associate Editor for the IEEE JOURNAL OF SOLID-STATE CIRCUITS from 2006 to 2011, the IEEE TRANSACTIONS ON CIRCUITS AND SYSTEMS I from 2007 to 2009 and has been serving since 2016, and the IEEE TRANSACTIONS ON CIRCUITS AND SYSTEMS II from 2005 to 2007 and from 2012 to 2015.



Kei May Lau (S'78–M'80–SM'92–F'01) received the B.S. and M.S. degrees in physics from the University of Minnesota, Minneapolis, MN, USA, and the Ph.D. degree in electrical engineering from Rice University, Houston, TX, USA.

She was a faculty member of the Electronic and Computer Engineering Department, University of Massachusetts/Amherst, MA, USA, where she focused on metal-organic chemical vapor depositions, compound semiconductor materials, and devices programs. Since 2000, she has been with the Electronic and Computer Engineering Department, The Hong Kong University of Science and Technology, Hong Kong, where she is currently a Fang Professor of Engineering. She established the Photonics Technology Center for research in III-V materials, optoelectronics, high power and high-speed devices at HKUST.

Dr. Lau was a recipient of the U.S. National Science Foundation Faculty awards for Women Scientists and Engineers in 1991, the Croucher Senior Research Fellowship in 2008, and the IEEE Aron Kressel Award in 2017. She is an Editor of the IEEE EDL and an Associate Editor of the *Applied Physics Letters*.